GEOPHYSICAL RESEARCH LETTERS, VOL. 36, L21402, doi:10.1029/2009GL039672, 2009

Pan arctic terrestrial snowmelt trends (1979–2008) from spaceborne passive microwave data and correlation with the Arctic Oscillation

M. Tedesco,[1,2] M. Brodzik,[3] R. Armstrong,[3] M. Savoie,[3] and J. Ramage[4]

Received 19 June 2009; revised 18 August 2009; accepted 15 September 2009; published 5 November 2009.

[1] We report pan-arctic terrestrial snowmelt trends for the period 1979 – 2008 derived from spaceborne microwave brightness temperature (Tb) and study the correlation between these trends and the Arctic Oscillation (AO). Melting is detected using a spatially and temporally dynamic algorithm using the difference between daytime and nighttime Tb values (Diurnal Amplitude Variations, DAV). Results indicate statistically significant negative trends for melt onset and end dates as well as for the length of the melt season. On the average, over the past 30 years melt has been starting (finishing) ~0.5 days/year (~1 days/year) earlier and the length of the melting season is shortening by ~0.6 days/year. Results indicate that the AO index variability can explain up to 50% of the melt onset variability over Eurasia and only 10% of that over North America, consistent with spatial patterns of surface temperature changes related to the AO. **Citation:** Tedesco, M., M. Brodzik, R. Armstrong, M. Savoie, and J. Ramage (2009), Pan arctic terrestrial snowmelt trends (1979–2008) from spaceborne passive microwave data and correlation with the Arctic Oscillation, *Geophys. Res. Lett.*, *36*, L21402, doi:10.1029/2009GL039672.

1. Introduction and Rationale

[2] Melting snow can be mapped by means of spaceborne microwave brightness temperatures (Tbs) [e.g., *Mote et al.*, 1993; *Drobot and Anderson*, 2001; *Ramage*, 2001; *Tedesco*, 2007; *Takala and Pulliainen*, 2008], continuously collected at a global scale since 1979 [*Knowles et al.*, 2002; *Armstrong et al.*, 1994] as the appearance of liquid water within the dry snowpack suddenly and abruptly increases microwave Tb [e.g., *Tedesco et al.*, 2006]. Many of these algorithms use daily (or multiple days) averaged Tb, which may increase the uncertainty on the estimated melt onset dates (MODs) and melt end dates (MEDs). One of the proposed methodologies, however, makes use of data collected during both ascending and descending passes (diurnal amplitude variations, DAV) [e.g., *Ramage and Isacks*, 2002; *Tedesco*, 2007], hence improving the temporal resolution of the derived MODs and MEDs. In the DAV approach histograms of Tbs (measured during both dry and wet snow conditions) can be modeled by means of a bimodal distribution, with the left (right) normal distribution, LND (RND), containing Tb representative of dry (wet) snow conditions. Wet snow is assumed to occur when measured Tb belongs to the RND (e.g., Tb is greater than a threshold value *Tc*) and the DAV is greater than a threshold value *DAVc*. During dry snow conditions, the DAV is relatively low but it considerably and abruptly increases when melting begins. To account for those cases when both ascending and descending Tbs are high, snow is flagged as wet when both ascending and descending Tbs are greater than *Tc* [*Tedesco*, 2007].

[3] In this study, we use a modified version of the original DAV-based algorithm [e.g., *Ramage and Isacks*, 2002] to study trends of MODs, MEDs and of the melt season length, between 1979 and 2008 for areas at latitudes above 60°N. Previously published studies are either focusing on a specific area [*Takala and Pulliainen*, 2008] or on a shorter period [*Wang et al.*, 2008]. The major change of the new DAV algorithm here used is that both *Tc* and *DAVc* are dynamically computed, for each year and pixel. We have therefore named the new algorithm Dynamic-DAV (D-DAV) and the version previously reported in the literature Static-DAV (S-DAV). Microwave data consists of vertically polarized Tb at Ka band measured between 1978 and 1987 by the Scanning Multichannel Microwave Radiometer (SMMR, 37 GHz) [*Knowles et al.*, 2002] and by the Special Sensor Microwave/Imager (SSM/I, 1987–2008, 36.5 GHz) [*Armstrong et al.*, 1994] between 1987 and 1991 (F-08 satellite), 1991 and 1995 (F-11) and 1995 – 2008 (F13). Sensor cross-calibration is necessary and is performed following *Jezek et al.* [1991] for the SMMR to SSM/I F08 calibration, *Abdalati et al.* [1995] for the F11 to F08 sensors and *Stroeve et al.* [1998] for the F11 and F13 sensors. The gaps in the SMMR time series of Tb consequent to the smaller SMMR swath with respect to that of SSM/I are filled with values computed by linear interpolation from adjacent days. The overpass times of the SSM/I sensors are similar, with ascending (descending) equatorial crossing time for the SSM/I sensors on the F-8 satellite at dawn (dusk) and dusk (dawn) for the ones on the F-11 and F-13 satellites. However the ascending (descending) equatorial crossing time for SMMR is local noon (midnight). The different crossing times between the SMMR and SSM/I sensors are a major source of uncertainty in the long-term trends of both MOD and MED. To quantify this uncertainty would require concurrent measurements during MODs and MEDs. Unfortunately, the overlapping period for the SMMR and SSM/I F-08 sensors occurs during July and August, when melting has already started or is already over. We can only speculate that, in view of the crossing time, SMMR might detect earlier (later) MOD (MED) than SSM/

[1] Earth and Atmospheric Sciences, City College of New York, City University of New York, New York, New York, USA.
[2] Joint Center for Earth Systems Technology, University of Maryland, Baltimore County, Baltimore, Maryland, USA.
[3] National Snow and Ice Data Center, Boulder, Colorado, USA.
[4] Earth and Environmental Sciences Department, Lehigh University, Bethlehem, Pennsylvania, USA.

0094-8276/09/2009GL039672$05.00

I, even if the relatively smaller SMMR Tbs with respect to SSMI (from the calibration regression formulas) could play the opposite role.

[4] Results from D-DAV are used to study the correlation between MODs and MEDs trends and the Arctic Oscillation (AO), defined as the leading mode of sea level pressure variability from an Empirical Orthogonal Function (EOF) analysis for the Northern Hemisphere winter [*Thompson and Wallace*, 1998]. Its major characteristics are a primary center of action over the Arctic and opposing weaker centers in the North Atlantic and North Pacific [*Serreze and Barry*, 2005]. *Rigor et al.* [2002] suggest that spring surface air temperature (SAT) anomalies over the Arctic Ocean are correlated with the AO index during previous winter. *Bamzai* [2003] uses maps of composite snow cover to indicate that winter season AO and winter/spring season snow cover are significantly correlated on seasonal time scales. Here we study if and how this correlation translates to the MODs and MEDs. This is not straightforward because other components of the surface energy balance beside SAT can affect melting.

2. D-DAV Algorithm

[5] In S-DAV, both *Tc* and *DAVc* are spatially and temporally fixed [e.g., *Ramage and Isacks*, 2002; *Tedesco*, 2007]. Differently, in the D-DAV approach, the threshold *DAVc* is computed as $DAV_c = DAV_{Jan.\ Feb.} + 10$ K, with $DAV_{Jan.\ Feb.}$ being the January-February DAV average. The value of *DAVc* used in the S-DAV is 10 K [*Ramage and Isacks*, 2002]. We introduced the $DAV_{Jan.\ Feb}$ offset because we observed that, for some pixels, DAV values during dry snow conditions could be as high as 12–14 K, with averaged January-February DAV values up to 6 K. The threshold *Tc* in D-DAV is computed modeling the bimodal distribution *B* describing the Tb histograms as $B(p, m_1, s_1, m_2, s_2) = p \cdot G(m_1, s_1) + (1 - p) \cdot G(m_2, s_2)$, where p is the percentage of dry pixels, G is a Gaussian distribution and m_i and s_i are, respectively, the mean and standard deviation of the ith normal distributions. For each pixel and year, the five parameters (p, m_1, s_1, m_2, s_2) are computed through a fitting procedure minimizing the mean square error between the values of the Tb histogram (January through August) and those of the bimodal distribution, using the Levenberg–Marquardt method. The optimal threshold value is then computed by minimizing the probability of erroneously classifying a dry pixel as a wet pixel and vice versa) as $T = (-B \pm (B^2 - 4AC))/2A$ with $A = s_1^2 - s_2^2$, $B = 2(m_1 \cdot s_2^2 - m_2 \cdot s_1^2)$ and $C = m_2^2 \cdot s_1^2 - m_1^2 \cdot s_2^2 + 2\, s_1^2 \cdot s_2^2 \cdot \ln(s_2 \cdot p/s_1 \cdot (1 - p))$ [*Gonzalez and Wintz*, 1987]. The value of T falling between m_1 and m_2 is the desired threshold *Tc*. For those cases when the fitting procedure does not converge, the threshold value on Tb is set to 255 K [*Tedesco et al.*, 2006]. Once *Tc* and *DAVc* are computed, melting is identified when both of the following conditions are met: C1) $DAV_i \geq DAV_c$ and C2) $Tb_i^P \geq Tb_{c.}$, with P being either Ascending or Descending and i the day of the year. Melting is also assumed to occur when C3) ($Tb_i^{Asc.} \geq Tb_{Threshold}$ and $Tb_i^{Desc.} \geq Tb_{Threshold}$), to account for melting that persist during nighttime [*Tedesco*, 2007]. The date of the end of the melt season is defined as the last day when $DAV_i \geq DAV_c$ and $Tb_i \geq Tc$.

[6] To evaluate the performance of the D-DAV algorithm at large spatial scales, we compared MODs and MEDs derived from QuikSCAT [*Wang et al.*, 2008] with those derived from D-DAV. Figure 1 shows the mean (2000 – 2006) MODs (Figure 1a) and MEDs (Figure 1b) derived with D-DAV and the difference between MODs derived from QuikSCAT and SSM/I using D-DAV (Figure 1c) and between the melt off dates from QuikSCAT and MEDs derived from D-DAV (Figure 1d), for the period 2000 – 2006. Histograms of the differences between MODs and MEDs obtained with QuikSCAT and D-DAV are also reported in Figures 1e and 1f. The values of the mean and standard deviation of the normal distributions fitting the two histograms are, respectively, 1.74 days and 1.12 days in the case of the MOD and −1.67 days and 2.93 days in the case of the MED. No evident spatial pattern related to features such as vegetation and elevation is observed. D-DAV detects MOD (MED) earlier (later) than QuikSCAT. The difference between the two algorithms might be due to the different cell grid size of the two data sets, to the different frequencies, and to the adopted threshold values.

[7] We also compared the outputs of the D-DAV algorithm with estimates of MODs and MEDs derived from the analysis of daily snow depth (SD) and SAT measured by 49 stations of the World Meteorological Organization (WMO) for three snow seasons (2003 through 2006, http://www.ncdc.noaa.gov). The stations used in this study and the related data set were previously used by *Tedesco and Miller* [2007], where they are fully described. Since we lack the required information to solve the surface energy balance equations and compute the snow temperature, we assumed that melting occurs when SAT is exceeding 0 °C. The correlation between MODs from D-DAV and those estimated from Ts for all stations and years is $R^2 = 0.8$ with a mean absolute error of 4.8 days and a standard deviation of 8.6 days. During our analysis, we noted that D-DAV can indicate melting when SAT is still below but close to 0 °C. Possible explanations include different spatial scales at which the two data sets are acquired, the presence of subsurface melting (not identified by SAT analysis) and the fact that WMO stations report the 2m air temperature rather than the actual snow temperature. Following *Wang et al.* [2008], we also studied the histograms of SAT one and two days before and on the same day when melting is identified by D-DAV. The number of SAT occurrences above 0 ° C was 10% two days before the identified melting date, 29% one day before and 65% on the date when melting is estimated by the D-DAV algorithm. The shift in the staistical distribution of SAT from largely below freezing to above freezing during the estimated D-DAV melt date confirms that the D-DAV algorithm is sensitive to the melt onset signal. When comparing the date of the last day of melting from D-DAV and the date of snow disappearance from snow depth measurements, we found a correlation of $R^2 = 0.4$, with a mean error (over all samples) of 14 days and a standard deviation of 12 days. We point out here that comparing the D-DAV MEDs with the snow disappearance dates from WMO data has intrinsic problems. As pointed out by *Wang et al.* [2008], WMO stations do not report a 'zero' snow depth for days when there is no snow but rather a flag value (*9999*), also corresponding to missing data. Moreover, the

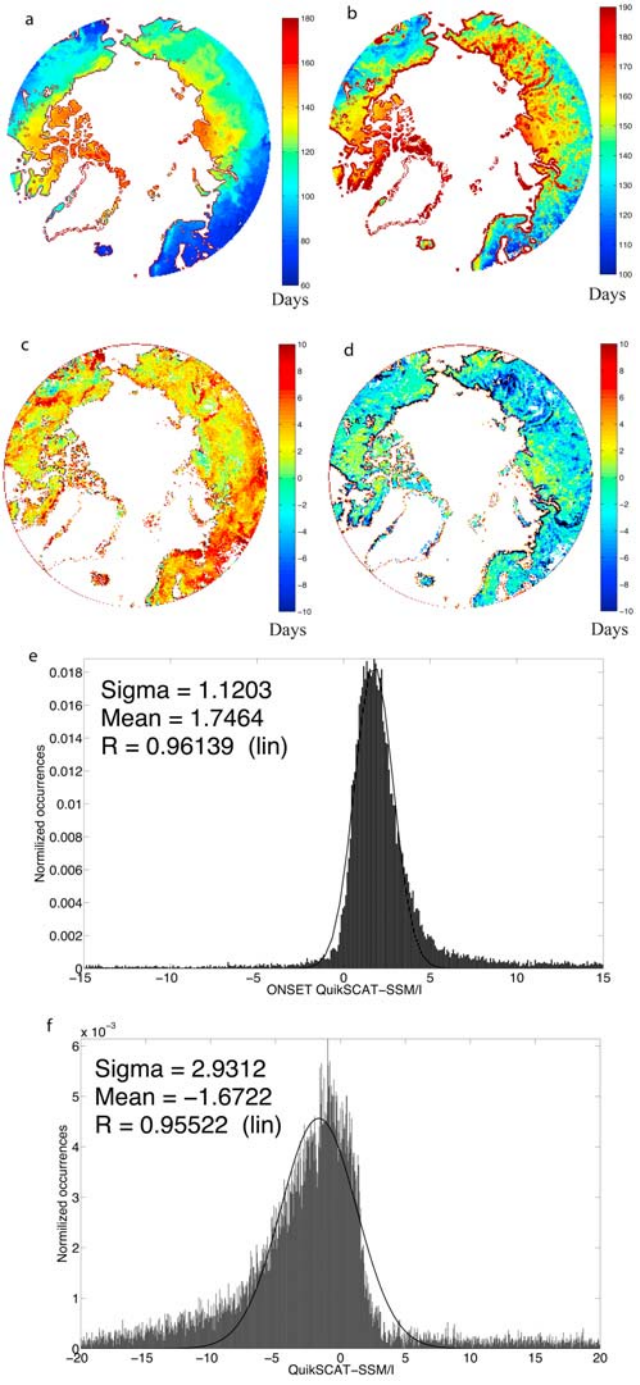

Figure 1. Maps of average (2000–2006) (a) melt onset and (b) refreeze dates derived with the D-DAV and differences between (c) MODs derived from QuikSCAT and SSM/I using D-DAV [Days] and (d) melt off dates from QuikSCAT and melt end date from SSM/I and D-DAV, averaged for the seasons 2000 through 2006. (e–f) The histograms of the differences are also reported together with the mean and standard deviation values of the normal distributions fitting the histograms.

MED computed by the D-DAV might differ from the actual date of snow disappearance.

3. Results and Discussion

[8] Figure 2 shows the maps of (a) melt onset and (d) melt end date trends together with (g) the trend of melt season duration, expressed in days/year and derived with D-DAV over the period 1979 – 2008. Negative values of the MOD (MED) trends suggest that melting is starting (ending) earlier. A negative trend of the melt season duration means that the melt season is shortening. Not all trends are statistically significant ($p < 0.1$), as observable from the maps of p-values in Figures 2b, 2e, and 2h, where areas with $p > 0.1$ are masked in black. In the case of MODs (MEDs), the pixels with statistically significant trends at the 90% level are ~78% (91%), becoming ~75% in the case of the melt season length. Elevated p-values of the melt onset trends in east Eurasia occur over areas with high elevations, but this is not happening for the remaining areas of Eurasia and North America, where we did not find significant correspondence between the distribution of p-values and either elevation or forest cover fraction. The mean and the standard deviation of the histograms of statistically significant trends (Figures 2c, 2f, and 2i) are fitted with Gaussian distributions (black line). The mean and standard deviation of the Gaussian distribution for MODs (MEDs) are, respectively, −0.47 (−0.97) days/year and 0.14 (0.38) days/year. In the case of the melt season length we obtain a mean of −0.43 days/year and a standard deviation of 0.17 days/year. The histograms also show that all statistically significant MODs trends are negative. Most of the MEDs trends and melt season length are negative, with the exception of a small subset showing positive values.

[9] For each year, we computed the average value of melt onset, melt end dates and melt season duration for areas where statistically significant trends are obtained and for subset areas including North America or Eurasia and studied the correlation with AO during the period 1979 – 2008. The standardized anomalies (1979 – 2008 as a baseline) of the spatially averaged values are reported in Figure 3. Here black bars refer to the spatial average over the entire study area, 50% gray bars to North America (NA) and 25% gray bars to Eurasia (EU). The January through March averaged AO index (http://www.cdc.noaa.gov/data/correlation/ao.data) is also reported in Figure 3a (black line with circles). The trends derived from linear regression analysis for the spatially averaged MODs (MEDs) are −0.47 days/year (−0.97 days/year) for the whole area, −0.46 days/year (−0.94 days/year) for Eurasia and −0.43 days/year (−0.94 days/year). The trends in the case of the spatially averaged melt season length are −0.52 days/year for the whole area, −0.49 days/year for Eurasia and −0.55 days/year for North America.

[10] From Figure 3 we observe that positive melting-related anomalies in 1979 and the beginning of the 1990's appear to be associated with the persistent negative phase of AO during the same period. MOD anomalies become generally negative after the 1990s, when the AO went from a strongly negative to a positive state. The correlation between MODs and JFM AO indices (1979 – 2008) is $R = -0.62$, hence explaining about 36% of the melt onset

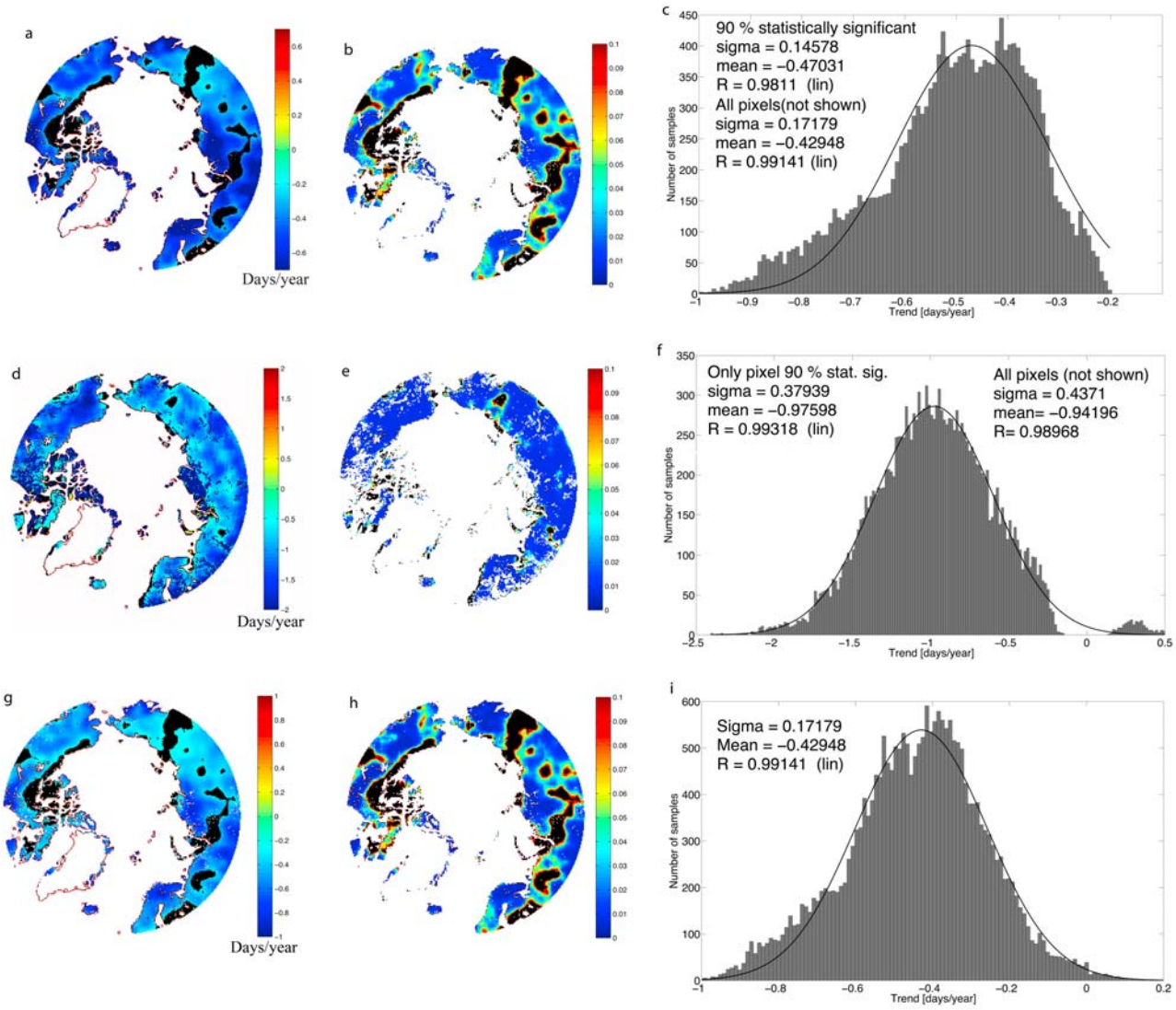

Figure 2. Maps of D-DAV derived (a) melt onset, (d) melt end date trends, and (g) melt season duration [Days/year] for the period 1979–2008 together with the maps of p-values for the (b) melt onset, (c) melt end date, and (h) melt season length. The histograms of statistically significant (at 90% level) trend values in the case of melt onset (Figure 2c), melt end dates (Figure 2f) and melt season duration (Figure 2i) are also reported together with the Gaussian distributions (black line) fitting the histograms.

variability over the whole study area. The AO variability, however, explains ∼50% (R = −0.7) of melt onset variance over Eurasia but less than 10% (R = −0.25) of the North America MOD variability. Results are 99% statistically significant for the whole area and Eurasia, but not for North America (with a p-value of 0.16). The anti-correlation between AO and MOD trends is consistent with the correlation between spring SAT anomalies and AO index over the Arctic Ocean [*Rigor et al.*, 2002] and with the results reported by *Kryjov* [2002], suggesting that more than 50% of the 30 year (1968–97) trends in both winter and spring SAT for northwestern Russia and more than 40% for northwestern Siberia are linearly correlated with the winter AO. The poor correlation between AO and North America melt onset variability is consistent with the spatial patterns of the SAT anomalies related to AO: strong positive changes in January through March surface temperatures congruent with AO extend across Northern Eurasia, smaller response are observed over eastern United States and negative responses are found over eastern Canada and southern Greenland [*van Loon and Rogers*, 1978; *Serreze and Barry*, 2005]. The correlation between MED trends and AO was not found to be statistically significant over the whole region and Eurasia, but it was statistically significant over North America (at 95% level), though poor, with R = −0.34. This suggests that the effect of AO on snowmelt does not propagate through the length of the melting season so that it can affect the MED trends.

4. Conclusions

[11] Applying the D-DAV algorithm to spaceborne microwave Tbs collected between 1979 and 2008 we found that statistically significant negative trends exist for the MODs, MEDs and for the length of the melting season. Our results indicate that, on the average, for the past 30 years

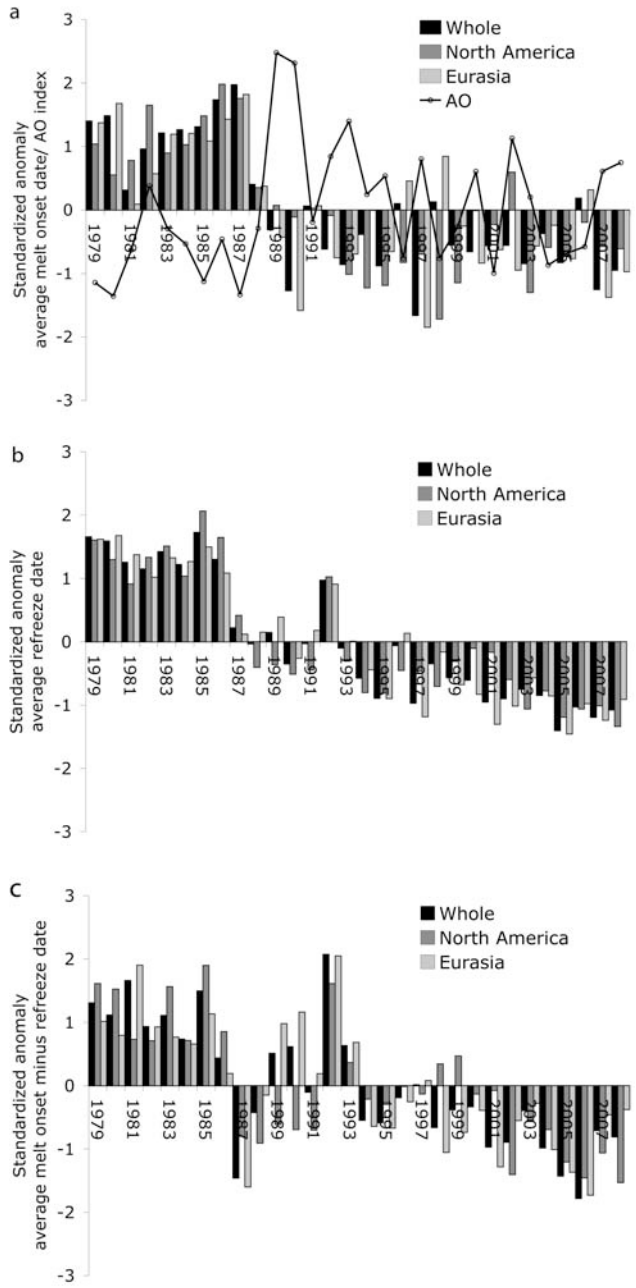

Figure 3. Standardized anomaly (1979–2008) of spatially averaged (a) melt onset, (b) melt end dates, and (c) melt season length for the whole area (black bars), for North America (NA, 50% gray) and Eurasia (EU, 25% gray). The January through March averaged AO indices are reported as a black line with circles in Figure 3a.

melting for areas above 60°N has been starting and ending sooner and that the length of the melting season has shortened. The trends of MOD (MED) range between −0.2 (−2.4) days/year and −1.8 (0.8) days/year, with a spatially averaged trend of ∼−0.47 days/year (−0.97 days/year). Results also indicate that the melting season has been shortening by −0.57 days/year, consistently with recently observed warming in the Arctic region. The AO index variability explains up to 50% of the melt onset variability over Eurasia but only 10% of that over North America, consistently with spatial patterns of surface temperature anomalies correlated with the AO index. Over the whole region under study, the AO index could explain ∼36% of the MODs variability. Not statistically significant or poor correlation values were found when considering the AO index with MEDs and melt season duration. The MED and MOD trends not explained by the AO might be linked to other factors such as changes in long-term snow albedo, in the surface energy balance terms (related to changes in clouds) or to SAT warming trends not correlated to AO, Recent years have seen a shift of AO toward a more neutral state. If a new negative regime develops, it will be crucial to monitor if this will lead to cooling or will be superimposed on a more general warming trend.

[12] **Acknowledgments.** The authors wish to thank Libo Wang and Chris Derksen (Environment Canada) for the QuikSCAT results and the National Snow and Ice Data Center and the NOAA Climate Diagnostics Center for providing the Tb and AO datasets, respectively. This work was supported by the NASA Terrestrial and Hydrology Program and the Cooperative Institute for Research and Environmental Sciences (CIRES). This work was supported by the National Aeronautics and Space Administration (NASA) and the Cooperative Institute for Research and Environmental Sciences (CIRES).

References

Abdalati, W., K. Steffen, C. Otto, and K. C. Jezek (1995), Comparison of brightness temperatures from SSMI instruments on the DMSP F8 and F11 satellites for Antarctica and the Greenland ice sheet, *Int. J. Remote Sens.*, *16*, 1223–1229, doi:10.1080/01431169508954473.

Armstrong, R. L., K. W. Knowles, M. J. Brodzik, and M. A. Hardman (1994), DMSP SSM/I Pathfinder Daily EASE-Grid Brightness Temperatures, http://nsidc.org/data/nsidc-0032.html, Natl. Snow and Ice Data Cent., Boulder, Colo.

Bamzai, A. S. (2003), Relationship between snow cover variability and Arctic Oscillation index on a hierarchy of time scales, *Int. J. Climatol.*, *23*, 131–142, doi:10.1002/joc.854.

Drobot, S., and M. Anderson (2001), An improved method for determining melting onset dates over Arctic sea ice using scanning multichannel microwave radiometer and Special Sensor Microwave/Imager data, *J. Geophys. Res.*, *106*, 24,033–24,049, doi:10.1029/2000JD000171.

Gonzalez, R. C., and R. Wintz (1987), *Digital Image Processing*, Addison-Wesley, Reading, Mass.

Jezek, K. C., C. Merry, D. Cavalieri, S. Grace, J. Bedner, D. Wilson, and D. Lampkin (1991), Comparison between SMMR and SSM/I passive microwave data collected over the Antarctic Ice Sheet, *Tech. Rep. 91-03*, Byrd Polar Res. Cent., Columbus, Ohio.

Knowles, K. W., E. G. Njoku, R. L. Armstrong, and M. Brodzik (2002), Nimbus-7 SMMR Pathfinder Daily EASE-Grid Brightness Temperatures, http://nsidc.org/data/nsidc-0071.html, Natl. Snow and Ice Data Cent., Boulder, Colo.

Kryjov, V. (2002), The influence of the winter Arctic Oscillation on the northern Russia spring temperature, *Int. J. Climatol.*, *22*, 779–785, doi:10.1002/joc.746.

Mote, T. L., M. R. Anderson, K. C. Kuivinen, and C. M. Rowe (1993), Passive microwave-derived spatial and temporal variations of summer melt on the Greenland ice sheet, *Ann. Glaciol.*, *17*, 233–238.

Ramage, J. M. (2001), Satellite remote sensing of daily, seasonal, and annual changes on southeast Alaskan glaciers 1986–1998, Ph.D. dissertation, Cornell Univ., Ithaca, N. Y.

Ramage, J. M., and B. L. Isacks (2002), Determination of melt-onset and refreeze timing on southeast Alaskan icefields using SSM/I diurnal amplitude variations, *Ann. Glaciol.*, *34*, 391–398, doi:10.3189/172756402781817761.

Rigor, I. G., J. M. Wallace, and R. L. Colony (2002), Response of sea ice to the Arctic Oscillation, *J. Clim.*, *15*, 2648–2663, doi:10.1175/1520-0442(2002)015<2648:ROSITT>2.0.CO;2.

Serreze, M., and R. Barry (2005), *The Arctic Climate System*, Cambridge Univ. Press, Cambridge, U. K.

Stroeve, J., L. Xiaoming, and J. Maslanik (1998), An intercomparison of DMSP F11- and F13-derived sea ice products, *Remote Sens. Environ.*, *64*, 132–152, doi:10.1016/S0034-4257(97)00174-0.

Takala, M., and J. Pulliainen (2008), Detection of snow melt using different algorithms in global scale, in *Microwave Radiometry and Remote Sensing of the Environment, 2008*, doi:10.1109/MICRAD.2008.4579496, Inst. of Electr. and Electr. Eng., New York.

Tedesco, M. (2007), Snowmelt detection over the Greenland ice sheet from SSM/I brightness temperature daily variations, *Geophys. Res. Lett.*, *34*, L02504, doi:10.1029/2006GL028466.

Tedesco, M., E. J. Kim, A. W. England, R. D. De Roo, and J. P. Hardy (2006), Brightness temperatures of snow melting/refreezing cycles: Observations and modelling using a multilayer dense medium theory-based model, *IEEE Trans. Geosci. Remote Sens.*, *44*, 3563–3573, doi:10.1109/TGRS.2006.881759.

Tedesco, M., and J. Miller (2007), Observations and statistical analysis of combined active–passive microwave space-borne data and snow depth at large spatial scales, *Remote Sens. Environ.*, *111*, 382–397.

Thompson, D. W. J., and J. M. Wallace (1998), The Arctic Oscillation signature in the wintertime geopotential height and temperature fields, *Geophys. Res. Lett.*, *25*, 1297–1300, doi:10.1029/98GL00950.

van Loon, H., and J. C. Rogers (1978), The seesaw in winter temperatures between Greenland and northern Europe. Part I: General description, *Mon. Weather Rev.*, *106*, 296–310, doi:10.1175/1520-0493(1978)106<0296:TSIWTB>2.0.CO;2.

Wang, L., C. Derksen, and R. Brown (2008), Detection of pan-arctic terrestrial snowmelt from QuikSCAT, 2000–2005, *Remote Sens. Environ.*, *112*, 3794–3805, doi:10.1016/j.rse.2008.05.017.

R. Armstrong, M. Brodzik, and M. Savoie, National Snow and Ice Data Center, Boulder, CO 80309-0449, USA.

J. Ramage, Earth and Environmental Sciences Department, Lehigh University, Bethlehem, PA 18015, USA.

M. Tedesco, Earth and Atmospheric Sciences, City College of New York, City University of New York, New York, NY 10031, USA. (mtedesco@sci.ccny.cuny.edu)